First-principles study of interface effects on coercivity in Nd-Fe-B sintered magnets

学位論文（要約）

First-principles study of interface effects on coercivity in Nd-Fe-B sintered magnets

（Nd-Fe-B 焼結磁石における保磁力への界面効果に関する第一原理的研究）

平成２６年１２月　博士（理学）申請

東京大学大学院理学系研究科
物理学専攻

見澤　英樹

Abstract

The Nd-Fe-B sintered magnet has been widely used in application because of their high coercivity and magnetization. Importance of the Nd-Fe-B sintered magnets has increased in recent years because of spread of electric vehicles. However, the mechanism of the coercivity of the Nd-Fe-B sintered magnets is not revealed. There is a difficulty to understand the coercivity of the magnets because the magnets are not single crystals and they have a property, which comes from a multi-scale interface.

Their high coercivity is due to the large magnetic anisotropy of Nd atoms, but the coercivity of the actual Nd-Fe-B sintered magnets is not as high as expected theoretically from the magnetic anisotropy of Nd atoms. This gap is an interesting problem for application and theoretical study. One of proposed mechanisms for the coercivity is based on a picture of nucleation of a reversed magnetic domain in interfaces of $Nd_2Fe_{14}B$ main phase and sub-phase. Recent experimental study indicates that the microstructure of the sub-phases can enhance the coercivity.

In this thesis, we focus on Nd oxides as the sub-phases to develop a basis for Dy-free magnets. We investigate the property of the interface of $Nd_2Fe_{14}B$ main phase and Nd-oxide sub-phase by the first-principles calculation to understand the mechanism of the enhancement of the coercivity. We determine the stable structure of the interface between $Nd_2Fe_{14}B$ with Nd oxides with various oxygen concentration. With the optimized structure, we calculate magnetic anisotropy energies of interfacial Nd atoms and discuss a dependence of the magnetic anisotropy on the positions of the interfacial oxygen atoms. We evaluate the coercivity of the interface using the Landau-Lifshitz-Gilbert equation with parameters derived from first-principles study. Lastly, From the above results we establish a mechanism for the enhancement of the coercivity.

Acknowledgements

First and foremost, I would like to express my deepest gratitude toward my supervisor, Professor Shinji Tsuneyuki, for his teaching on physics from a broad perspective and his insightful suggestion for this work. Without his encouragement, this work would not be possible. I am also deeply grateful to Associate Professor Yoshihiro Gohda for his strict teaching on physics and on the manner of acting as a researcher. Also, I express my deep appreciation toward Assistant Professor Ryosuke Akashi for sparing much time for teaching me on the scientific writing. I am grateful to Dr. Daisuke Hirai and Dr. Yasutomi Tatetsu for discussion on the permanent magnets. I really appreciate all the members of Tsuneyuki research group. I also appreciate Ms. Emi Shimoshikiryo for many paperworks on my research activity.

Part of this work has been supported by the Elements Strategy Initiative Center for Magnetic Materials under the outsourcing project of MEXT. The computations were partly performed on the K-computer at the RIKEN Advanced Institute for Computational Science (Project No. hp120086) and supercomputers at ISSP, The University of Tokyo.

Contents

Chapter 1

Introduction

1.1 Importance of Nd-Fe-B sintered magnets

The Nd-Fe-B sintered magnet has been invented in 1982 by M. Sagawa (published in 1984 [1, 2]), and has been the most powerful class of magnets up to now. There has been a surprising growth of production of Nd-Fe-B sintered magnets because they are composed of low-cost elements and plentiful in nature compared with other high performance magnets. Thanks to advances in the technology of sintering magnets, the energy product $(BH)_{max}$, which is the performance measure of the permanent magnets, reached 85 % of theoretical limit in 2000 [3]

The energy product $(BH)_{max}$is mainly determined by the coercivity H_c and remanence M_r. The coercivity is defined by the magnitude of magnetic field which is needed to reverse the direction of macroscopic magnetic moments of magnetic materials, whereas the remanence denotes the magnetization when the applied field is reduced to zero after the material is magnetized.

After the beginning of the 21st century, the demand for the magnets with high coercivity has increased because of the rapid spread of the hybrid electric vehicles, which need the powerful motors. Figure 1.1 shows the energy product $(BH)_{max}$ and the coercivity of (Nd,Dy)-Fe-B sintered magnets with the operating temperature [4]. As seen in Figure 1.1, by substituting Dy atoms for Nd atoms, the coercivity of Nd-Fe-B sintered magnets is increased, but their $(BH)_{max}$ decrease due to the decrease of the magnetization. The

operating temperature for the hybrid electric vehicles is approximately 200°C. therefore approximately 30 % of Nd atoms needs to be substituted by Dy atoms.

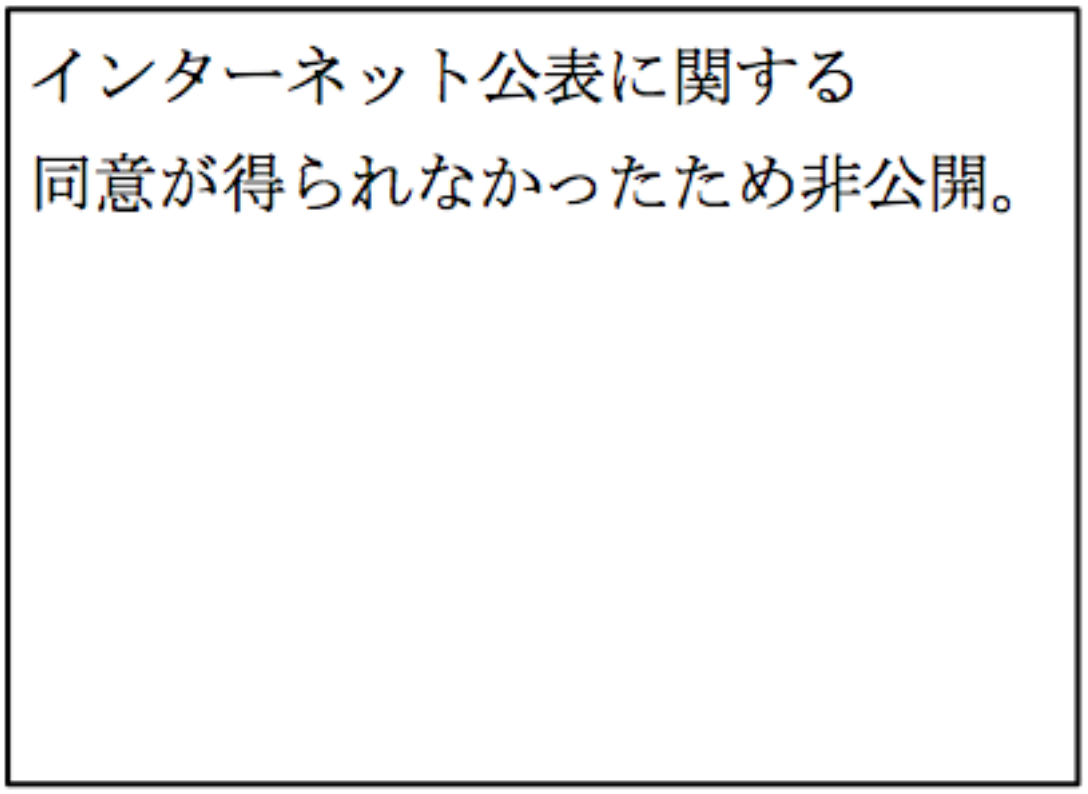

FIGURE 1.1:
$(BH)_{max}$ of (Nd,Dy)-Fe-B sintered magnets.
(This figure is taken from [4])

The Dy-substitution into Nd-Fe-B sintered magnets have some problems. Firstly, the energy product $(BH)_{max}$ becomes smaller as Nd is replaced with Dy due to the anti-ferromagnetic coupling between Dy and Fe moments. Secondly, Dy is a scarce natural resource and therefore its sustainable supply is difficult. Because of this drawbacks, Dy-free high coercivity magnets are in great demand and the interest in the coercivity mechanism of Nd-Fe-B sintered magnets has revived recently.

1.2 General theory of the coercivity

Here, we introduce the simplest view of the coercivity in the single-domain particles.

1.2.1 Magnetic ion in the crystal

The interaction between electrons in the $4f$ orbitals and the electric field generated by the charge from the surrounding electrons can be expressed by the following crystal field Hamiltonian [5]

$$H_{\mathrm{cf}} = \sum_{n,m} A_n^m \langle r^n \rangle \theta_n^J O_n^m(\vec{J}) \tag{1.1}$$

where $\vec{J}$ is the total angular momentum of the atoms. A_n^m is the crystal field parameter which describes the effect of the surrounding charge. θ_n^J and $O_n^m(\vec{J})$ are the Stevens factor and the Stevens operator which are dependent only on the kind of magnetic ions and not affected by the crystal field. $\langle r^n \rangle$ denotes an expectation value of r^n for the radial part of $4f$ wave function.

According to the Hund's rule, the electronic charge shows anisotropic distribution. For example, $4f$ electrons in Gd^{3+} show isotropic charge distribution as depicted in Figure 1.2. On the other hand, $4f$ electrons in Nd^{3+} and Dy^{3+} show anisotropic charge distribution. Such electronic distribution governs the Stevens factor and operator for the respective ions. In particular, the distributions in Nd^{3+} and Dy^{3+} yield negative 2nd order Stevens factors.

インターネット公表に関する
同意が得られなかったため非公開。

FIGURE 1.2:
Charge distribution of $4f$ electrons: Gd^{3+},Nd^{3+}, and Dy^{3+}
(This figure is taken from [6].)

1.2.2 Magnetic anisotropy energy of materials with $4f$ and $3d$ electrons

The $4f$ electrons around rare-earth ions in permanent magnets are strongly localized and therefore the rare-earth ions can be considered as localized magnetic moments having anisotropic charge distributions in a crystal field.

The effective Hamiltonian for the $4f$ electrons is expressed by the following expression [7]

$$H_{\text{eff}} = \lambda L_{4f} \cdot S_{4f} - 2H_{\text{exc}} \cdot S_{4f} + V_{\text{cf}} \tag{1.2}$$

where $S_{4\text{f}}$ and $L_{4\text{f}}$ are the $4f$ spin and orbital moment. λ is the spin-orbit coupling constant. The first term is the spin-orbit coupling between the $4f$ spin moment and the $4f$ orbital moment. The second term is the exchange magnetic coupling between the $4f$ electrons of the rare-earth atom and the $3d$ electrons of Fe atoms. The last term represents the effects of the crystal field interaction, which interact with the anisotropic charge density of the $4f$ electrons and this term is the origin of anisotropy of the total system.

In $Nd_2Fe_{14}B$, the first term is much larger ($\sim 10^3$K) than others ($\sim 10^2$K). Since Nd^{3+} has positive λ, the spin moment and the orbital moment are fixed in the opposite directions. As a result, the total angular momentum of Nd^{3+} is $J = |L - S| = |6 - \frac{3}{2}| = \frac{9}{2}$ with respect to the direction of the orbital moment. The second term is expressed by

$$2H_{\text{exc}} \cdot S_{4f} = J_{\text{eff}} S_{3d} \cdot S_{4f}, \tag{1.3}$$

where J_{eff} is the effective exchange constant between the $3d$ spin moment of Fe and the $4f$ spin moment of Nd. J_{eff} is negative in $Nd_2Fe_{14}B$ because of the exchange interaction. In this way, the total moment of Nd^{3+} points in the same direction as that of Fe. Finally, the crystal field gives the anisotropic energy depending on the direction of the magnetic moment of Nd^{3+} and the total moments of the system.

In $Dy_2Fe_{14}B$, since λ of Dy^{3+} is positive, the total moment of Dy^{3+} points in the direction opposite to that of the $3d$ moment of Fe. This is the reason that the energy product BH_{max} decreases with the Dy-substitution.

1.2.3 Magnetocrystalline anisotropy

Single crystals of ferromagnetic materials have anisotropic properties dependent on the direction of magnetic moment when magnetized. For example, the single crystal of Fe is easily magnetized along with $\langle 100 \rangle$ direction, and is hardly magnetized along with $\langle 111 \rangle$ direction. The axis which can be magnetized easily is called "easy axis", whereas the one which is hardly magnetized is called "hard axis". The materials which have only one easy axis are classified as "materials with a uniaxial magnetic anisotropy".

The total energy of the materials with the uniaxial magnetic anisotropy $E_{\mathrm{A}}^{\mathrm{total}}$ in the ferromagnetic phase is described as

$$E_{\mathrm{A}}^{\mathrm{total}} = K_1^{\mathrm{total}} \sin^2\theta + K_2^{\mathrm{total}} \sin^4\theta + K_3^{\mathrm{total}} \sin^6\theta + \cdots \tag{1.4}$$

where θ is the angle between the easy axis and the direction of the macroscopic magnetic moments. K_n^{total} is the magnetocrystalline constant of nth order.

Similarly, the energy of the magnetic ion such as Nd in $Nd_2Fe_{14}B$ can be described as

$$E_{\mathrm{A}}^{i} = K_1^{i} \sin^2\theta_i + K_2^{i} \sin^4\theta_i + K_3^{i} \sin^6\theta_i + \cdots \tag{1.5}$$

where i is the index of magnetic atoms. θ_i is the angle between the easy axis and the direction of the magnetic moment of the atom i. K_n^i is the magnetic anisotropy constant of the atom i of nth order. In this thesis, we consider only the first-order term:

$$E_{\mathrm{A}}^{i} = K_1^{i} \sin^2\theta_i \tag{1.6}$$

1.2.4 Coercivity of a particle with single magnetic domain

Suppose a magnetic field is being applied to a ferromagnetic material in the direction opposite to the macroscopic magnetic moment. When the field is rather strong, the direction of the moment is reversed. The basic model to express this magnetic reversal is the Stoner-Wohlfarth model, which is based on the picture that the reversal occurs as rotation of the macroscopic magnetic moments of the isolated single domain particle. When the single magnetic domain particle with the uniaxial magnetic anisotropy is in

the external magnetic field, the total energy of the particle is expressed by

$$U = K_1 \sin^2\theta - M_s H_{ext} \cos\phi \tag{1.7}$$

where θ is the angle between the easy axis and the magnetic moment, and ϕ is the angle between the magnetic moment and the external magnetic field. M_s is the magnitude of the magnetic moment of the particle, and H_{ext} is the magnitude of the external field. We assume that directions of the moments are initially set in the direction of the easy axis

For the external field parallel to the easy axis, namely $\phi = \theta$, the moment in the initial direction ($\theta = 0$) is unstable when the following condition is met.

$$\frac{\partial^2 U}{\partial \theta^2} = 2K_1 \cos 2\theta + M_s H_{ext} \cos\theta \leq 0 \tag{1.8}$$

Solving this equation, we can see that the magnetic field which is able to reverse the moment is

$$H_A = -\frac{2K_1}{M_s} \tag{1.9}$$

This external field is called as the anisotropic magnetic field, and this has been believed to be the theoretical maximum value of the coercivity in the literature [8].

1.3 Coercivity of $Nd_2Fe_{14}B$ sintered magnets

The actual $Nd_2Fe_{14}B$ sintered magnets is more complicated than the single domain model assumed in the Stoner-Wohlfarth theory because they are neither the single magnetic domain particle nor the single crystal. Figure 1.3 shows a typical back-scattered electron scanning electron microscopy image of the sintered Nd-Fe-B magnet. As seen from Figure 1.3, this magnet is composed of crystal grains of $Nd_2Fe_{14}B$ and sub-phases, namely, grain boundary phase and Nd-rich phases. The Nd-rich phases has been suggested to be various phases such as metallic fcc Nd and Nd oxides. [4]

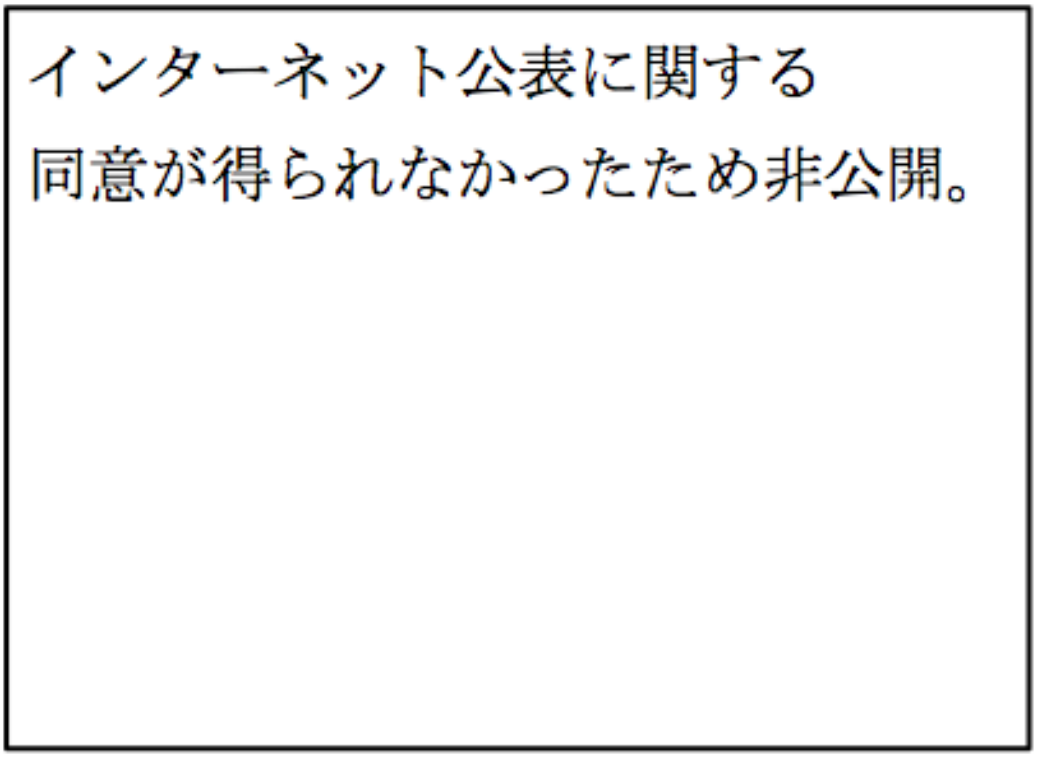

FIGURE 1.3:
High-resolution back-scattered electron (BSE) scanning electron microscopy (SEM) image of a sintered Nd-Fe-B permanent magnets
(This figure is taken from [4])

It is well known that the coercivity of the Nd-Fe-B sintered magnet is sensitive to the microstructure of the grain-boundary phases [9–12]. Considering the dependency of the coercivity on the microstructure, various mechanisms of the coercivity of the Nd-Fe-B sintered magnet have been proposed. Among them, we here introduce the nucleation mechanism. [8]

In the nucleation mechanism, the coercivity is defined by the magnetic field which create the reversed domain at the interface of the crystal grain and sub-phases (Figure 1.4). First, in the interface region, whose magnetic moments are subject to the sub-phase, a reverse of magnetic moments occurs. Since the energy of the reversed domain is governed only by the volume of the domain wall, the domain propagates to the internal region of the crystal grain without increase of energy. After repeating the reversal and propagation, all the moments in the main phase become reversed.

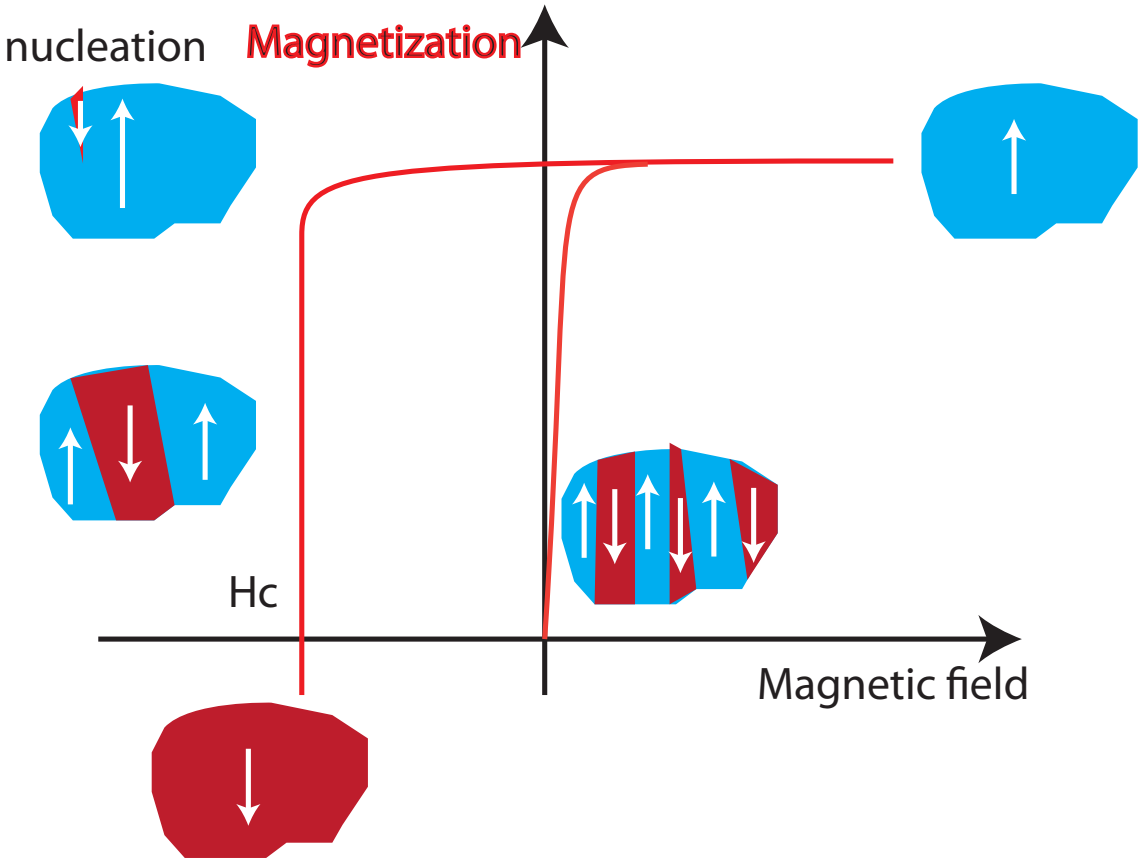

FIGURE 1.4: Schematic picture of demagnetization curve based on the nucleation process.

For the enhancement of the coercivity, it is therefor needed to suppress the nucleation of the reversed domain. Some methods have been proposed to suppress the nucleation. One approach for suppressing the nucleation is the Dy-substitution of Nd atoms at the interface of the crystal grain of $Nd_2Fe_{14}B$ [13, 14]. As expected from Figure 1.1, the local coercivity of the interface of the crystal grains is enhanced, and the nucleation is suppressed. Figure 1.5 shows the demagnetization curves of the untreated and Dy-diffusion-processed $Nd_2Fe_{14}B$ sintered magnets [14]. The coercivity of Dy-diffused sample increases largely, and this result suggests that the nucleation of the reversed domain at the interface is the key factor of the coercivity.

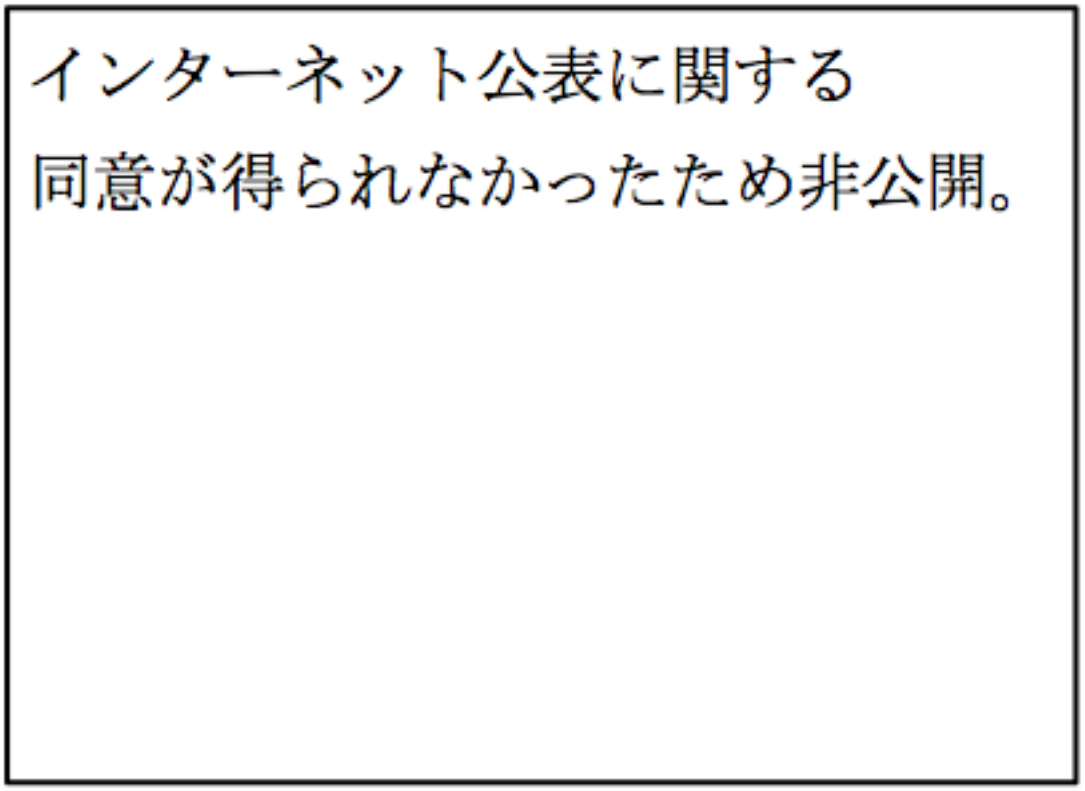

FIGURE 1.5:
Demagnetization curves of the untreated and Dy diffusion processed samples
(This figure is taken from [14])

Recently, the enhancement of coercivity by the post-sinter annealing has been reported in many experiments [15–18]. Particularly, We focused on the experiment where the enhancement of the coercivity of $Nd_2Fe_{14}B$ films by the oxidation of the Nd has been observed [19]. Because Dy is not needed in this approach, this method is a desirable approach for the enhancement of the coercivity. Figure 1.6 shows the demagnetization curves of the $Nd_2Fe_{14}B$ films. When the $Nd_2Fe_{14}B$ films are coated with Nd and annealed at 550 °C, the coercivity is substantially enhanced. This result shows that the oxidation of the Nd has an important role in the suppression of the nucleation of the reversed domain. In this experiment, the observed Nd oxides has the fcc structure, and its oxygen concentration is approximately 16 at%. Table 1.1 show the results of Energy-dispersive X-ray spectroscopy quantitative analysis of fcc Nd oxides.

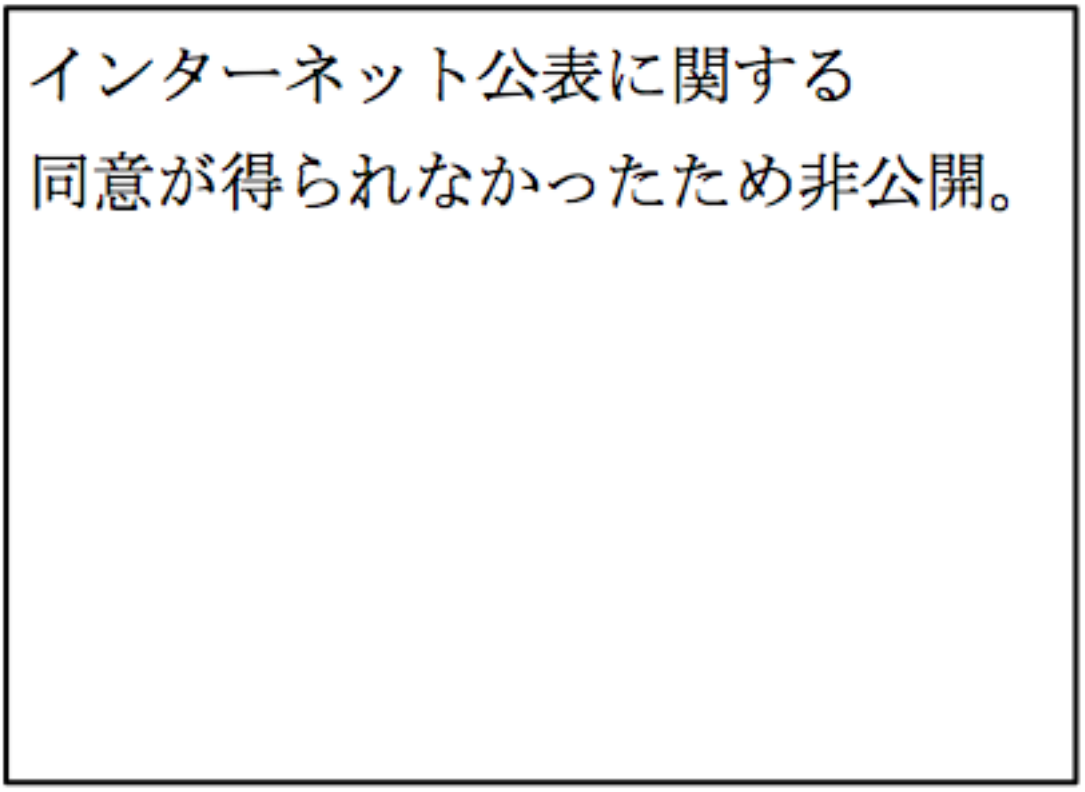

FIGURE 1.6:
Effect of oxidation of Nd layer on coercivity recovery
(This figure is taken from [19])

TABLE 1.1: Energy-dispersive X-ray spectroscopy quantitative analysis of fcc Nd oxides. the data is taken from [19]

	at%
O(K_α)	15.76
Fe(K_α)	5.98
Nd(L_α)	78.24

1.4 Former works for the coercivity of $Nd_2Fe_{14}B$ sintered magnets

There are some approaches to evaluate the coercivity of the Nd-Fe-B sintered magnets. A typical approach is micromagnetic simulation, which is based on the Landau-Lifshitz-Gilbert equations[20, 21]. Figure 1.7 shows an example of the micromagnetic simulations based on a finite element method [22–24]. Sub-micron sized $Nd_2Fe_{14}B$ grains are modeled as rectangular shapes. Such simulations can reproduce demagnetization curves of NdFeB particles qualitatively. However, with this approach, we cannot consider atomic-scale effects, especially interface effects between $Nd_2Fe_{14}B$ main phases and sub-phases. In this thesis, we consider atomic-scale effects of the interface between $Nd_2Fe_{14}B$ main phases and sub-phases, using a first-principles calculation to investigate a quantitative property.

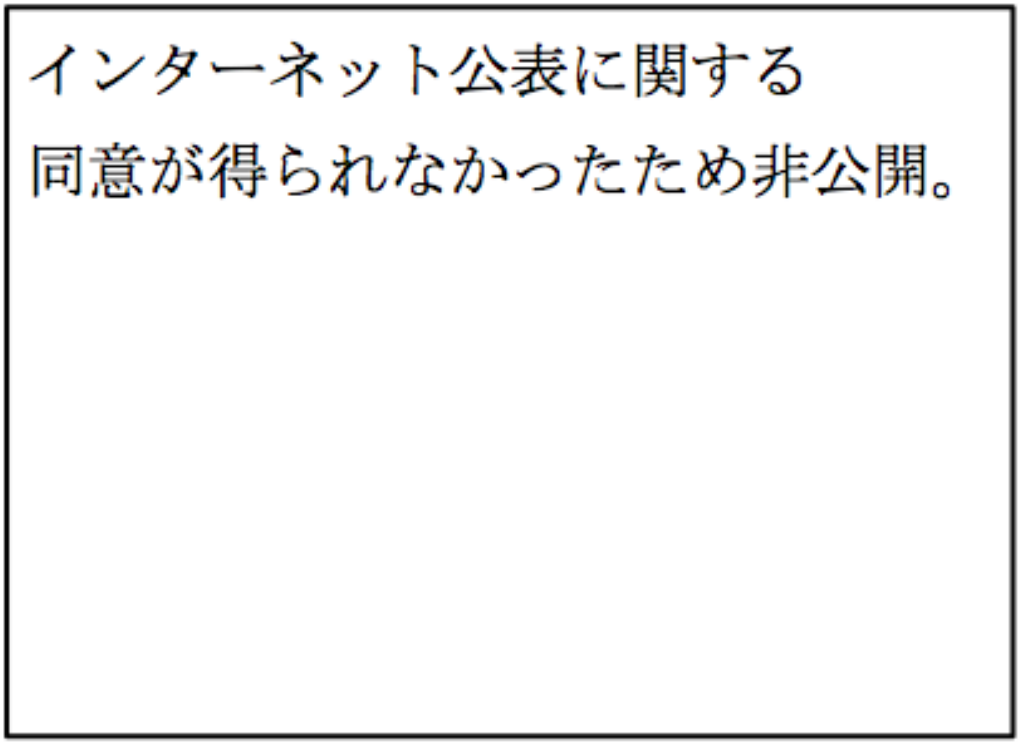

FIGURE 1.7:
(a) Demagnetizing factor(N) dependence of demagnetization curves. (b) mesh size dependence of demagnetization curves. (c) Images of magnetic reversal process. (This figure is taken from [22])

1.5 Motivation of the study and the outline of the thesis

The demand of the Dy-free high coercivity magnets has risen in recent years. If the effect of the oxidation of the Nd sub-phase on the suppression of the magnetic reversal is clarified, it may lead to a Dy-free method to synthesize powerful magnetic materials.

The first-principles theoretical studies for $Nd_2Fe_{14}B$ have been done by some researchers [25–28], and the magnetic anisotropy on the surface of $Nd_2Fe_{14}B$ main phase has been investigated in the first-principles study [29, 30]. However, studies on the magnetic anisotropy of the realistic interface explicitly treating $Nd_2Fe_{14}B$ main phase and Nd-oxide sub-phase has not been performed. In this study, we investigate the effects of the realistic interface between $Nd_2Fe_{14}B$ and Nd oxides on the coercivity by the first-principles study and the goal is the development of a basis for future proposal of the high coercivity Dy-free permanent magnets.

This thesis is organized as follows. Firstly, we introduce the calculation methods in Chap. 2. Next, in Chap. 3, we study the bulk form of the main phase and sub-phase to develop a basis for the latter calculations. In Chap. 4, we calculate the optimized structure of the interface and discuss the stable positions of the interfacial oxygen atoms. Using the derived optimum structure, we evaluate the magnetic anisotropy energy of the interfacial Nd atoms in Chap. 5. In Chap. 6. we investigate the interfacial effects on coercivity with the results in previous chapter. Finally, we conclude this work in Chap.7.

Chapter 2

Methods

In this chapter, we introduce the calculation methods used in our work. Firstly, the density functional theory is briefly reviewed. We use the density functional theory to determine the optimized structure for the evaluation of the magnetic anisotropy. Secondly, the method to evaluate the magnetic anisotropy energy is introduced. Thirdly, the method to evaluate the coercivity based on the Landau-Lifshitz-Gilbert equation is introduced, where the magnetic anisotropy energy calculated in the second step is employed.

2.1 Density functional theory

2.1.1 Hohenberg-Kohn theorem

The many-body wave functions of electrons obey the Schrödinger equation.

$$\mathcal{H}\left|\Phi\right\rangle = (T_{\mathrm{e}} + U_{\mathrm{ee}} + V_{\mathrm{ei}})\left|\Phi\right\rangle = E\left|\Phi\right\rangle \tag{2.1}$$

where,

$$T_{\mathrm{e}} = \sum_{\sigma} \int dr \psi_{\sigma}^{\dagger}(r)(-\frac{\Delta}{2})\psi_{\sigma}(r) \tag{2.2}$$

$$U_{\mathrm{ee}} = \frac{1}{2}\sum_{\sigma,\sigma'} \int dr \int dr' \psi_{\sigma}^{\dagger}(r)\psi_{\sigma'}^{\dagger}(r')\frac{1}{|r-r'|}\psi_{\sigma'}(r')\psi_{\sigma}(r) \tag{2.3}$$

$$V_{\mathrm{ei}} = \sum_{\sigma} \int dr \psi_{\sigma}^{\dagger}(r) (\sum_{i} \frac{Z_i}{|R_i - r|}) \psi_{\sigma}(r) \tag{2.4}$$

This many-body Schrödinger equation can not be solved analytically in general solids. However, in 1964 [31], P. Hohenberg and W. Kohn have proved two important theorems, which are the bases of the density functional theory.

First, they have proved that there is a one-to-one correspondence between the electron density and the external field with respect to the ground states.

$$n(r) \iff V_{\mathrm{ei}} \quad \text{(in the ground state)} \tag{2.5}$$

Second, they have proved that there is a variational principle with respect to the electron density.

$$E[n(r)] = \langle \Phi_0[n(r)] \,|\, T_{\mathrm{e}} + U_{\mathrm{ee}} + V_{\mathrm{ei}} \,|\, \Phi_0[n(r)] \rangle \tag{2.6}$$

$$E[n(r)] \geq E[n_0(r)] = E_0 \tag{2.7}$$

These statements assure that the ground states of electrons are obtained by minimizing the energy as a functional of the electron density.

2.1.2 Kohn-Sham equations

On the basis of the Hohenberg-Kohn theorems, W. Kohn and L. Sham developed a practical one-electron self-consistent eigenvalue equations (the Kohn-Sham equation) [32]. In the Kohn-Sham approach, the many-body electron system is mapped to an auxiliary non-interacting electron system. The complicated interactions of many-body system are then handled by the exchange-correlation functional as a functional of the electron density.

The Kohn-Sham energy, which is the variational energy functional of the auxiliary system, can be expressed in

$$E_{\mathrm{KS}}[n(r)] = T_s[n(r)] + \frac{1}{2} \int \int dr dr' \frac{n(r) n(r')}{|r - r'|} + \int dr n(r) V_{\mathrm{ei}}(r) + E_{\mathrm{xc}}[n(r)] \tag{2.8}$$

where

$$n(r) = \sum_{\sigma} \sum_{i=1}^{N_\sigma} |\psi_i^{\sigma}(r)|^2 \tag{2.9}$$

$$T_s[n(r)] = -\frac{1}{2}\sum_{\sigma}\sum_{i=1}^{N_\sigma}|\nabla\psi_i^\sigma(r)|^2 \tag{2.10}$$

The minimization of E_{KS} with respect to $\psi_i^{\sigma *}(r)$ leads to following eigenvalue equations.

$$\left[-\frac{1}{2}\nabla^2 + \int dr' \frac{n(r')}{|r-r'|} + V_{\mathrm{ei}}(r) + \frac{\delta E_{\mathrm{xc}}(r)}{\delta n}\right]\psi_i^\sigma = \epsilon_i^\sigma \psi_i^\sigma \tag{2.11}$$

And the total energy of the interacting system can be expressed in terms of these eigenvalues as follows.

$$E_{\mathrm{total}} = \sum_{\sigma,i}\epsilon_i^\sigma + E_{\mathrm{xc}} - \sum_\sigma \int dr n(r,\sigma)V_{\mathrm{ec}}^\sigma(r) - \frac{1}{2}\int\int dr dr' \frac{n(r)n(r')}{|r-r'|} \tag{2.12}$$

where E_{xc} is the exchange-correlation functional and $V_{\mathrm{ec}}^\sigma(r) = \frac{\delta E_{\mathrm{xc}}}{\delta n(r,\sigma)}$. Various exchange-correlation functionals have been proposed. In this work, we use Generalized Gradient Approximation (GGA) [33, 34] for the exchange-correlation functional.

2.1.3 DFT+U method

It is difficult to handle strongly localized electrons like $4f$ electrons with the GGA exchange-correlation functional because the approximation is based on an assumption that the electron density is nearly uniformly distributed, which is the nature of itinerant electron systems. To improve the accuracy of the calculation for the strongly correlated systems, the Hubbard-like additional functional has been proposed [35, 36]. We employ the functional proposed by Dudarev *et al* [36].

The DFT+U energy functional is:

$$E_{\mathrm{DFT+U}} = E_{\mathrm{DFT}} + E_{\mathrm{U}} \tag{2.13}$$

$$E_{\mathrm{U}} = \frac{U_{\mathrm{eff}}}{2}\sum_\sigma (n_{m,\sigma} - n_{m,\sigma}^2) \tag{2.14}$$

where $n_{m,\sigma}$ is the occupation number of the mth localized state, and σ is the spin index. This additional term is small when the occupation number of the localized state is near 0 or 1, therefore this term can be regarded as the penalty functional for the itinerant electrons.

2.1.4 Frozen core approximation

Another reliable method to calculate the system with $4f$ electrons is the frozen core approximation [37]. In the frozen core approximation, the Coulomb potential of the localized electrons is replaced with an effective Coulomb potential interacting only with the valence electrons. This approximation makes the cost of calculation lower, but sometimes it fails to produce correct electronic states with $4f$ electrons. In Chap. 3. we check the effectiveness of the approximation for our target system comparing with the DFT+U method.

2.2 Evaluation of magnetic anisotropy constant

In Chap. 1, we introduced the crystal field Hamiltonian Eq. (1.1) and the magnetic anisotropy constant Eq.(1.6). Using them, we here derive the specific form of K_1 for Nd^{3+}.Employing the lowest-order approximation for the Hamiltonian [38], we get

$$\mathcal{H}_{\rm cf} = A_2^0\langle r^2\rangle\theta_2^J O_2^0(\vec{J}), \tag{2.15}$$

where θ_2^J is $-\frac{7}{3^2 11^2}$ for Nd^{3+} ion. The expectation value of the Stevens operator for the state $|J,M\rangle$ can be expressed by

$$\langle J,M|\, O_2^0(\vec{J})\,|J,M\rangle = 2J(J-\frac{1}{2}) - 3J(J-\frac{1}{2})\sin^2\theta, \tag{2.16}$$

where θ is the angle of quantization axis of $\vec{J}$. The energy expectation value of the crystal field Hamiltonian is

$$\langle J,M|\,\mathcal{H}_{\rm cf}\,|J,M\rangle = A_2^0\langle r^2\rangle\theta_2^J\left(2J(J-\frac{1}{2}) - 3J(J-\frac{1}{2})\sin^2\theta\right). \tag{2.17}$$

Comparing Eq. (2.17) with Eq. (1.6), we determine the magnetic anisotropy constant for the atom by

$$K_1 = -3J(J-\frac{1}{2})\theta_J A_2^0\langle r^2\rangle \tag{2.18}$$

$$\langle r^2\rangle A_2^0 = \frac{1}{4}\int d\vec{R}(3\cos^2\theta - 1)\rho(\vec{R})\int dr 4\pi r^2 \frac{r_<^2}{r_>^3}\rho_{4f}(r) \tag{2.19}$$

where $r_<$ and $r_>$ are $\min(r, |\vec{R}|)$ and $\max(r, |\vec{R}|)$ respectively. $\rho(\vec{R})$ is the charge distribution except the $4f$ electrons and $\rho_{4f}(r)$ is the charge distribution of the $4f$ electrons These charges are determined with the first-principles calculation.

$\langle r^2 \rangle A_2^0$ is called the crystal field parameter, since θ_J is negative in Nd^{3+}, the magnetic anisotropy energy is proportional to the crystal field parameter.

2.3 Evaluation of the coercivity

2.3.1 Landau-Lifshitz-Gilbert equation

The Landau-Lifshitz-Gilbert (LLG) equation is a powerful tool for understanding dynamics of spin systems. [20, 21]. Considering the dynamics of one magnetic moment under an external magnetic field with the Zeeman term. The Hamiltonian is

$$\mathcal{H}_{\text{Zeeman}} = -\gamma_0 S \cdot H(t), \tag{2.20}$$

where $\gamma_0 = \frac{g\mu_B\mu_0}{\hbar}$ is the gyromagnetic constant. S is the spin operator and $H(t)$ is the external magnetic field. From the time-dependent Schrödinger equation, the expectation value of the spin operator follows

$$\frac{d}{dt}\langle S(t) \rangle = \gamma_0 \langle S(t) \rangle \times H(t). \tag{2.21}$$

Defining the magnetization by $M = \langle S(t) \rangle$, one can write the equation (2.21) for the magnetization as

$$\frac{dM}{dt} = -\gamma_0 M(t) \times H(t). \tag{2.22}$$

Eq. (2.22) yields the precession solution. In practice, damping term is phenomenologically introduced to obtain the static solution of the spin systems [39]. The resulting equation of motion is:

$$\frac{dM}{dt} = -\gamma_0 M \times H + \frac{\alpha}{|M|} M \times \frac{dM}{dt}, \tag{2.23}$$

where α is the Gilbert damping factor, and here we neglected the magnetostatic term. This damping term suppress the precession of a magnetic moment. Since we focus only on the final state ($t \to \infty$) , we treat α as an arbitrary parameter.

2.3.2 Atomic scale LLG scheme

In the later calculations with the LLG equation, Nd and Fe atoms are considered to be localized magnetic moments. For the ith atom, the equation is

$$\frac{dM_i}{dt} = -\gamma M_i \times H_i^{\text{eff}} + \frac{\alpha}{|M_i|} M_i \times \frac{dM_i}{dt}, \tag{2.24}$$

where H_i^{eff} is the effective magnetic field, which is derived by taking the derivative of the total energy with respect to the magnetic moment. Total energy of the system is defined as

$$E = \sum_i \left(-K_i (\hat{A}_i \cdot \hat{M}_i)^2 - \sum_j J_{ij} \hat{M}_i \hat{M}_j - H_{\text{ext}} \cdot \hat{M}_i \right), \tag{2.25}$$

where i is a site index, $\hat{A}_i$ is the easy axis of the atom, $\hat{M}_i$ is the normalized magnetic moment, K_i is the magnetic anisotropy constant, and J_{ij} is the exchange constant between moments. The first term denotes the magnetic anisotropy, the second term denotes the exchange coupling between the moments and the third term denotes the interaction with the external magnetic fields. Taking the derivative of total energy with respect to the magnetic moment, we get

$$H_i^{\text{eff}} = -\frac{\partial E}{\partial M_i} = \frac{2K_i}{|M_i|} (\hat{A}_i \cdot \hat{M}_i) \hat{A}_i + \sum_j \frac{J_{ij}}{|M_i|} \hat{M}_j + H^{\text{ext}}. \tag{2.26}$$

2.3.3 Flowchart of the evaluation of the coercivity

Figure 2.1 shows the flowchart of the evaluation of the coercivity. Firstly, we determine the optimized atomic position and the charge distribution of the interface of $Nd_2Fe_{14}B$ and Nd oxides. Next, we evaluate the Magnetic anisotropy energy of the interfacial Nd atoms from the position and charge obtained in previous calculations. Lastly, we evaluate the coercivity of the interface to use the LLG equations.

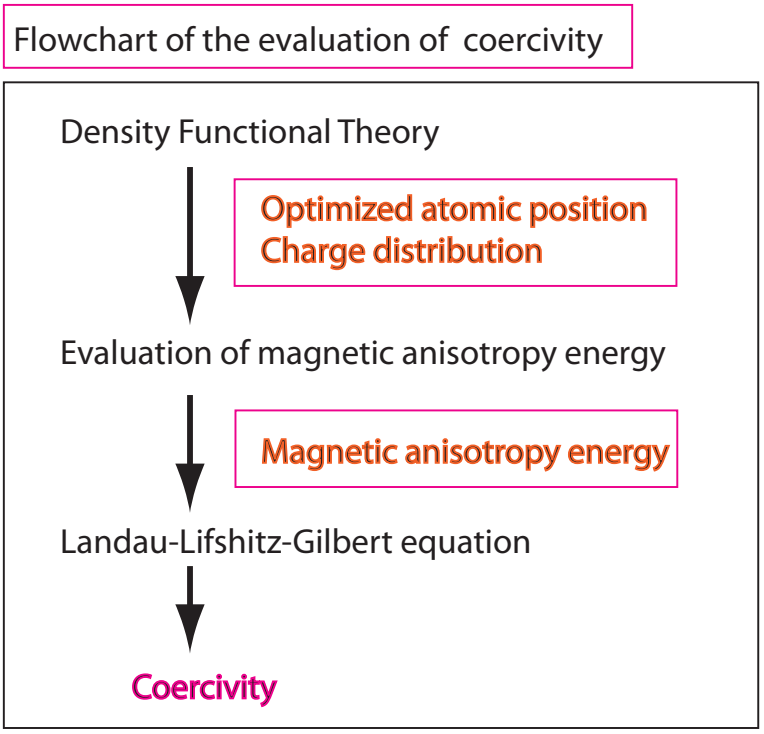

FIGURE 2.1: Flowchart of evaluation of coercivity

第３章

本章については、５年以内に

雑誌等で刊行予定のため、非公開。

第４章

本章については、５年以内に

雑誌等で刊行予定のため、非公開。

第５章

本章については、５年以内に

雑誌等で刊行予定のため、非公開。

第６章

本章については、５年以内に

雑誌等で刊行予定のため、非公開。

Chapter 7

Conclusions

In this thesis, we investigated the interface effects on the coercivity of $Nd_2Fe_{14}B$ sintered magnets based on the first-principles calculation. The aim of this study was to understand the effects of the oxidation of Nd atoms in the interface of $Nd_2Fe_{14}B$ main phase and Nd-oxide sub-phase on the coercivity.

Firstly, we calculated the electronic states and stable atomic configuration of the bulk form of the main phase and sub-phase to develop a basis for the later calculation and to check the effectiveness of the approximation used in the study. We found that the simple frozen core approximation is accurate enough to reproduce the result almost identical to that with the more sophisticated DFT+U approximation. In the calculation for the Nd-oxide sub-phase, we found that the fluorite structure is more stable than the rock-salt one. We thus established the stable structure of Nd oxides in the experimental situation where the enhancement of the coercivity has been observed.

For evaluation of the magnetic anisotropy, we next calculated the stable atomic positions of the interface of $Nd_2Fe_{14}B$ and Nd oxides in Chap. 4. In particular, we examined the positions of the oxygen atoms. From the evaluation of the defect formation energy of oxygen atoms, we found that they prefer interfacial sites near the Nd atoms in the main phase when the oxygen concentration is low.

In Chap.5, we calculated the magnetic anisotropy energy of Nd ions in the three structures for the $Nd_2Fe_{14}B$: bulk $Nd_2Fe_{14}B$, $Nd_2Fe_{14}B$-vacuum interface, and $Nd_2Fe_{14}B$-Nd oxides interface. We found that the magnetic anisotropy energy of interfacial Nd atoms

is very sensitive to the distance from the interfacial oxygen. When the $Nd_2Fe_{14}B$ main phase is exposed to the vacuum, the sign of magnetic anisotropy energy of interfacial Nd atoms is inversed from that of Nd deep in the bulk. On the other hand, when the main phase is faced with the sub-phase some of the oxygen atoms are located near the interfacial Nd atoms. Then, the electrons around the oxygen atoms approaches to the Nd atoms, with which the electronic distribution around the bulk Nd atom is partially recovered. Consequently, the positive magnetic anisotropy energies of the interfacial Nd atoms are realized.

In Chap.6, we investigated the spin dynamics of the interface using parameters from first-principles calculation to evaluate the coercivity. We found that when the magnetic anisotropy energies of the interfacial Nd atoms turn to homogeneously negative the coercivity drastically decrease regardless of their absolute values. This indicates that the coercivity is very sensitive to the sign of the magnetic anisotropy energy of the interfacial Nd atoms. Next, we calculated the coercivity of the interface where the Nd atoms having positive and negative anisotropy energies are inhomogeneously distributed, with which we include the effect of oxygen atoms near the interfacial Nd atoms. We found that as the ratio of the Nd sites having positive magnetic anisotropy energy is increased, the coercivity is substantially recovered. This result indicates that the significant recovery of the coercivity in the experiment is due to the oxidation in the interface region. Through this study, we established a reliable mechanism to enhance the coercivity of the magnets by interfacial oxygen atoms. The interfacial oxygen atoms, introduced by oxidation of metallic Nd sub-phase for example, change the magnetic anisotropy of interfacial Nd atoms from negative to positive. According to our view, the effects of oxygen atoms originate from the electronic charge around them. Therefore, we expect that the similar recovery of the coercivity is observed also by injecting atoms of other kinds. Even if all the interfacial Nd atoms do not have positive magnetic anisotropy, the recovery of the coercivity is significant. This idea can be verified by experiments with nitridization, fluoridation, and carbonization.

Appendix A

Effect of the magnetic anisotropy of Fe on a coercivity

We employed the magnetic anisotropy of Fe in the LLG equation in Chap. 6. As seen in Table 6.1 and Table 6.3, the magnetic anisotropy energy of Fe is smaller than that of Nd. We evaluated the coercivity of homogeneously modulated interfaces under the conditions without the magnetic anisotropy of Fe to investigate the effects of the magnetic anisotropy of Fe on the coercivity. The calculation condition is the same as that in section 6.1.

Figure A.1 shows the coercivity of the system with modulated interfacial magnetic anisotropy. The red points denote the coercivity of the interface with the magnetic anisotropy of Fe, while the blue points denotes the coercivity without the magnetic anisotropy of Fe.

We find that the coercivity is enhanced by 7% on average when the magnetic anisotropy of Fe is employed. Although the magnetic anisotropy of Fe is 0.3% of that of the internal Nd atoms on average, it affects largely the coercivity of the interface.

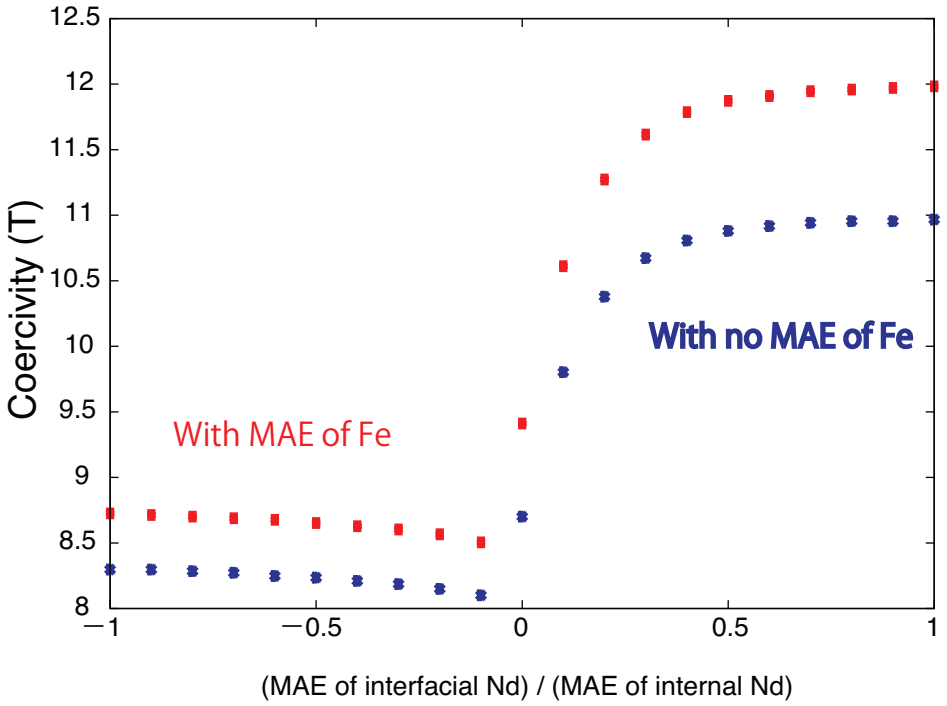

FIGURE A.1: Coercivity of the system with modulated interfacial magnetic anisotropy

Bibliography

[1] M. Sagawa, S. Fujiwara, N. Togawa, H. Yamamoto, and Y. Matsuura. *J. Appl. Phys.*, 55:2083, 1984.

[2] M. Sagawa, S. Fujiwara, H. Yamamoto, Y. Matsuura, and K. Hiraga. *IEEE Trans. Magn. Mag.*, 20:1584, 1984.

[3] Y. Kaneko, K Tokuhara, and Y. Sasakawa. *J. Jpn. Soc. Powder Powder Metall.*, 47:139, 2000.

[4] K. Hono and H. Sepehri-Amin. *Scripta Mater.*, 67:530, 2012.

[5] K. W. H. Stevens. *Proc. Phys. Soc*, A65:209, 1952.

[6] J. Sievers. *Z. Phys. B - Condensed Matter*, 45:289, 1982.

[7] J. Franse and R. Radwánski. *Handbook of Magnetic Materials, Vol. 6, ed. K. H. J. Buschow (Amsterdam: North-Holland)*, 1991.

[8] J. M. D. Coey. *Magnetism and magnetic materials (Cambridge university press)*, 2009.

[9] J. Liu, S. Hossein, T. Ohkubo, H. Hiki, A. Hattori, T. Schrefl, and K. Hono. *Acta Mater.*, 61:5387, 2013.

[10] H. Sepehri-Amin, Y. Une, T. Ohkubo, K. Hono, and M. Sagawa. *Scr. Mater.*, 65: 396, 2011.

[11] W. B. Cui, Y. K. Takahashi, and K. Hono. *Acta Mater.*, 59:7768, 2011.

[12] H. Sepehri-Amin, W. F. Li, T. Ohkubo, T. Nishiuchi, S. Hirosawa, and K. Hono. *Acta Mater.*, 58:1309, 2010.

[13] H. Nakamura, K. Hirota, M. Shimao, T. Minowa, and M. Honshima. *IEEE Trans. Magn.*, 41:3844, 2005.

[14] H. Sepehri-Amin, T. Ohkubo, and K. HOno. *J. Appl. Phys.*, 107:09A745, 2010.

[15] J. Fidler and J. Bernardi. *J. Appl. Phys.*, 70:6456, 1991.

[16] F. Vial, F. Joly, E. Nevalainen, M. Sagawa, K. Hiraga, and K. T. Park. *J. Magn. Magn. Mater.*, 242-245:1329, 2002.

[17] W. F. Li, T. Ohkubo, and K. Hono. *Acta Mater.*, 57:1337, 2009.

[18] H. Sepehri-Amin, T. Ohkubo, T. Shima, and K. Hono. *Acta Mater.*, 60:819, 2012.

[19] T. Fukagawa, T. Ohkubo, S. Hirosawa, and K. Hono. *J. Magn. Magn. Mater.*, 322: 3346, 2010.

[20] L. D. Landau and L. M. Lifshitaz. *Physik. Zeits. Sowjetunion*, 8:153, 1935.

[21] M. Lakshmanan. *Phil. Trans. R. Soc. A*, 309:1280, 2011.

[22] J. Thielsch, D. Suess, L. Schultz, and O. Gutfleisch. *J. Appl. Phys.*, 114:228909, 2013.

[23] P. Krone, D. Makarov, M. Albrecht, T. Schrefl, and D. Suess. *J. Magn. Magn. Mater.*, 322:3771, 2010.

[24] S. Bance, B. Seebacher, T. Schrefl, L. Exl, M. Winklhofer, G. Hrkac, G. Zimanyl, T. Shoji, M. Yano, N. Sakuma, M. Ito, A. Kato, and A. Manabe. *J. Appl. Phys.*, 116:233903, 2014.

[25] S. Tanaka, H. Moriya, H. Tsuchiura, A. Sakuma, M. Diviš, and P. Novák. *J. Phys.: COnf. Ser.*, 266:012045, 2011.

[26] X. B. Liu, Yilong Ma, Z. Altounian, Qiming Zhang, and J. Ping Liu. *J. Appl. Phys.*, 115:17A702, 2014.

[27] X. B. Liu and Z. Altounian. *J. Appl. Phys.*, 111:07A701, 2012.

[28] T. Suzuki, Y. Toga, and A. Sakuma. *J. Appl. Phys.*, 115:17A703, 2014.

[29] H. Moriya, H. Tsuchiura, and A. Sakuma. *J. Appl. Phys.*, 105:07A740, 2009.

[30] S. Tanaka, H. Moriya, H. Tsuchiura, A. Sakuma, M. Diviš, and P. Novák. *J. Appl. Phys.*, 109:07A702, 2011.

[31] P. Hohenberg and W. Kohn. *Phys. Rev.*, 136:B864, 1964.

[32] W. Kohn and L. J. Sham. *Phys. Rev.*, 140:A1133, 1965.

[33] D. C. Langreth and M. J. Mehl. *Phys. Rev. B*, 28:1809, 1983.

[34] A.D. Becke. *Phys. Rev. A*, 38:3098, 1988.

[35] A. I. Liechtenstein, V. I. Anisimov, and J. Zaane. *Phys. Rev. B*, 52:R5467, 1995.

[36] S. L. Dudarev, G. A. Botton, S. Y. Savrasov, C. J. Humphreys, and A. P. Sutton. *Phys. Rev. B*, 57:1505, 1998.

[37] G. B. Bachelet, D. R. Hamann, and M. Schlüter. *Phys. Rev. B*, 26:4199, 1982.

[38] M. Fähnle, K. Hummler, M. Liebs, and T. Beuerle. *Appl. Phys. A*, 57:67, 1993.

[39] T. L. Gilbert. *IEEE Trans. Magn.*, 40:3443, 2004.

[40] G. Kresse and J. Hafner. *Phys. Rev. B*, 47:558, 1993.

[41] G. Kresse. *Phys. Rev. B*, 59:1758, 1999.

[42] D. M. Ceperley and B.J. Alder. *Phys. Rev. Lett.*, 45:566, 1980.

[43] J. P. Perdew and A. Zunger. *Phys. Rev. B*, 23:5048, 1981.

[44] I. Kitagawa and Y. Asari. *Phys. Rev. B*, 81:214408, 2010.

[45] K. Hummler and M. Fähnle. *Phys. Rev. B*, 53:3290, 1996.

[46] Hong-Shuo Li, R. C. Mohanty, A. Raman, and C. G. Grenier. *J. Magn. Magn. Mater.*, 162:301, 1996.

[47] D. Givord and J. M. Moreau H. S. Li. *Solid State Commun.*, 50:497, 1984.

[48] D. Niarchos. *Hyperfine Interact.*, 49:367, 1989.

[49] T. Fukagawa, S. Hirosawa, T. Ohkubo, and K. Hono. *J. Appl. Phys.*, 105:07A724, 2009.

[50] URL http://exciting-code.org.

[51] S. Sagmeister and C. Ambrosch-Draxl. *Phys. Chem. Chem. Phys*, 11:4451, 2009.

[52] O. K. Andersen. *Phys. Rev. B*, 12:3060, 1975.

[53] H. Tsuchiura, Y. Toga, H. Moriya, and A. Sakuma. *Kotai butsuri (AGNE Gijutsu Center)*, 44:677, 2009.

[54] H. Moriya, H. Tsuchiura, and A. Sakuma. *J. Appl. Phys.*, 105:07A740, 2009.

[55] M. Yamada, H. Kato, H. Yamamoto, and Y. Nakagawa. *Phys. Rev. B*, 38:620, 1988.

[56] Z. Torbatian, T. Ozaki, S.Tsuneyuki, and Y. Gohda. *Appl. Phys. Lett.*, 104:242403, 2014.